JGR Atmospheres

RESEARCH ARTICLE
10.1029/2020JD033153

Special Section:
Atmospheric PM2.5 In China: Physics, Chemistry, Measurements, And Modeling

Establishment of Conceptual Schemas of Surface Synoptic Meteorological Situations Affecting Fine Particulate Pollution Across Eastern China in the Winter

Xuewei Hou[1], Bin Zhu[1], Kanike Raghavendra Kumar[2,1], Gerrit de Leeuw[1,3], Wen Lu[1], Qian Huang[1], and Xiaoxin Zhu[1]

[1]Collaborative Innovation Center on Forecast and Evaluation of Meteorological Disasters, Key Laboratory of Meteorological Disaster, Ministry of Education (KLME), Joint International Research Laboratory of Climate and Environment Change (ILCEC), School of Atmospheric Physics, Nanjing University of Information Science and Technology, Nanjing, China, [2]Department of Physics, Koneru Lakshmaiah Education Foundation (KLEF), Guntur, India, [3]R&D Satellite Observations, Royal Netherlands Meteorological Institute (KNMI), De Bilt, Netherlands

Abstract In the present study, the characteristics of weather conditions and local meteorological variables over the Beijing-Tianjin-Hebei (BTH) and the Yangtze River Delta (YRD) regions in the winter are analyzed using the principal component analysis (PCA) method and daily $PM_{2.5}$ accumulation rate. Typical synoptic weather patterns over China in the winter can be classified into four types. During the Type 1 synoptic weather pattern, China is under the influence of the Siberian High, and northerly winds prevail; this situation is beneficial to the transport of pollutants from north to south. However, when the Siberian High is weak, southerly winds prevail which may result in the transport of pollutants from south to north. The Type 2 weather pattern refers to a weak high pressure located in the BTH resulting in the accumulation of pollutants. During the Type 3 weather pattern, an intense cold Siberian High moves to the south and affects the northern areas of China. The associated front brings heavy precipitation in the YRD resulting in the wet deposition of pollution. During the Type 4 weather condition, the weak Siberian High is blocked by the northeast cold vortex and moves towards the south, causing the accumulation of pollution in the YRD. The PCA model shows that there are two transport pathways for pollutants to the BTH (YRD) area: one from the YRD (BTH) and Shandong during Types 1 and 2 (Types 1 and 3) situations and the other one from the central provinces during Type 4 (Types 1 and 4).

Key Points:
- The conceptual weather models for the accumulation and dissipation processes of fine particulate pollution are determined over East China
- The Siberian High winds reach China where the northerly winds prevailed with the transport of pollutants from north to south
- The weak Siberian High is blocked by the northeast cold vortex and moves towards the south and causes the accumulation of pollution

Supporting Information:
- Supporting Information S1

Correspondence to:
B. Zhu,
binzhu@nuist.edu.cn

Citation:
Hou, X., Zhu, B., Kumar, K. R., de Leeuw, G., Lu, W., Huang, Q., & Zhu, X. (2020). Establishment of conceptual schemas of surface synoptic meteorological situations affecting fine particulate pollution across eastern China in the winter. *Journal of Geophysical Research: Atmospheres*, *125*, e2020JD033153. https://doi.org/10.1029/2020JD033153

Received 23 MAY 2020
Accepted 22 OCT 2020
Accepted article online 31 OCT 2020

Author Contributions:
Conceptualization: Bin Zhu, Gerrit de Leeuw
Data curation: Wen Lu, Qian Huang
Formal analysis: Xuewei Hou
Investigation: Xuewei Hou
Methodology: Xuewei Hou, Kanike Raghavendra Kumar, Xiaoxin Zhu
Project administration: Bin Zhu
Resources: Kanike Raghavendra Kumar
Software: Xuewei Hou
(continued)

1. Introduction

In recent years, China has implemented active and effective measures to reduce air pollution, and the overall air quality has been improved significantly across the nation (Hou et al., 2019; Jin et al., 2016; Li et al., 2019). However, the concentrations of fine particulate matter ($PM_{2.5}$, i.e., the dry mass of aerosol particles with an aerodynamic diameter smaller than 2.5 μm) are often still high in some areas, especially in the Beijing-Tianjin-Hebei (BTH) and the Yangtze River Delta (YRD). The elevated $PM_{2.5}$ levels in these regions severely affect life and human health (Dang & Liao, 2019; Zhang et al., 2014, 2015). At the beginning of 2013, a large-scale and long-duration pollution event occurred over the eastern part of China (Tian et al., 2014; Wang, Zhang et al., 2014; Zhang et al., 2014). $PM_{2.5}$ concentrations as high as 772 $\mu g/m^3$ were observed in Beijing (Huang et al., 2014) and 300 $\mu g/m^3$ in Shanghai (Anderson et al., 2015). These values greatly exceed the health-based 24-hour air quality standard of 65 $\mu g/m^3$ given by the World Health Organization (WHO). This further strengthens the determination to improve air quality in China.

$PM_{2.5}$ represents a major environmental problem, causing reduced visibility, adverse effects on human health, and direct and indirect effects on weather and climate (Guo et al., 2014; Li et al., 2007; Wang et al., 2011, 2014). The spatial and temporal distributions of $PM_{2.5}$ concentrations in the atmosphere are affected by the direct emission of aerosols and their secondary formation from precursor gases, topographical conditions, and key meteorological factors (Hu et al., 2013). In the winter, severe $PM_{2.5}$ pollution days are frequently observed in China associated with an increased emission of pollutants, subsiding airflow in conditions with high atmospheric pressure, stagnant weather conditions, frequent inversions, and little precipitation (Wang, Yao, et al., 2014; Zhao et al., 2013; Zhang et al., 2016). Besides, the regional transport of

Supervision: Bin Zhu
Visualization: Xuewei Hou
Writing - original draft: Xuewei Hou
Writing – review & editing: Bin Zhu, Kanike Raghavendra Kumar, Gerrit de Leeuw

pollutants (Dang & Liao, 2019; Kang et al., 2019; Zheng et al., 2015, 2016) and the formation of secondary aerosols (Guo et al., 2014; Huang et al., 2014, 2018) have also made significant contributions to the intensification of pollution events.

Excessive emission is the underlying cause of frequent pollution, while meteorological conditions still play a vital role in the outbreak, maintenance, and dissipation of $PM_{2.5}$ pollution events (Cheng et al., 2011; Guo et al., 2017; He et al., 2009; Tai et al., 2012; Xu et al., 2003; Zhu et al., 2012). Adverse meteorological conditions, such as weak winds, strong inversions, and shallow mixing layers, seriously hinder the transportation and diffusion of pollutants out of the area, resulting in their local accumulation of pollutants (Feng et al., 2007; Huang et al., 2018; Kang et al., 2019; Ma et al., 2011; Miao et al., 2019; Pasch et al., 2011; Zhao et al., 2013, 2015). Moreover, the change of these local meteorological conditions is determined by the evolution of the daily weather, which is closely related to the large-scale weather situation (Ren et al., 2008; Wang et al., 2015; Wu et al., 2017; Zhang et al., 2014). Therefore, the identification and classification of large-scale weather situations lead to severe pollution episodes. Indeed, the analysis of their effects results in a better scientific understanding of processes leading to the formation of pollution and thus forecasting the occurrence of pollution events.

To evaluate the relationship between weather and air quality, we need multiple ways to define different weather patterns. The circulation-based classifications have become popular in climate and environmental studies, particularly in midlatitude and high-latitude regions where the day-to-day synoptic circulation variability dominates the local weather conditions (Huth et al., 2008; Jacobeit, 2010). This classification approach determines synoptic weather types from sea level pressure (SLP), geopotential height, or wind fields defined for each time interval of the analysis on a regular grid (Huth et al., 2008). This has been widely used to evaluate variations in the daily air quality (Bei et al., 2016, 2020; Comrie & Yarnal, 1992; Kalkstein & Corrigan, 1986; Li et al., 2019; Liu et al., 2020; McGregor & Bamzelis, 1995; Shahgedanova et al., 1998; Xu et al., 2016; Zhang et al., 2012). Zhang et al. (2012) used an objective classification method to identified nine weather types in Beijing from 2000 to 2009. They found that poor air quality is associated with a weak pressure field, with high pressure to the east, and low pressure to the northwest. Zhang et al. (2016) classified five categories of weather conditions based on the Kirchhofer method (El-Kadi & Smithson, 1992) by using the geopotential height at an altitude of 850 hPa during 1980–2013. The study showed that the strongest accumulation of air pollutants in the North China Plain occurred during a stagnant weather condition with stable conditions controlling most of the NCP with regional transport by westerly and southerly winds and local buildup. Xu et al. (2016) identified five synoptic weather types over Shanghai during the winters from 2013 to 2015. They reported that upstream transportation and poor diffusion conditions resulted in the highest $PM_{2.5}$ concentrations. Miao et al. (2017) identified seven synoptic weather types over the BTH region during summertime from 2011 to 2014. The results revealed that the synoptic patterns associated with massive aerosol pollution events are characterized by high-pressure systems located to the east or southeast of Beijing at the 925 hPa level. Similarly, Li et al. (2019) identified five typical synoptic weather patterns over the BTH during severe particulate pollution days during 2013–2018. Wang and Zhang (2020) identified six typical synoptic weather patterns in the BTH during the winters of 2013–2018. They demonstrated that the most dominant weather type (a cold high centered over the Xinjiang and Mongolian regions) in the BTH was also responsible for most of the severe particulate pollution days in the YRD. The number of weather types classified in the above studies is relatively large. Besides, the differences in weather conditions between clean days and polluted days are still not clear, which have important implications for emission control policy during different polluted levels.

The study mainly focused on the two city clusters, the BTH and YRD areas, where high pollution episodes occur in the winter. The atmospheric circulation influencing $PM_{2.5}$ concentrations was classified using a large amount of high spatial and temporal resolution data. The applicability of this classification was verified using six Siberian High indices (shown in the supporting information). We determined the conditions related to the primary weather conditions favorable to $PM_{2.5}$ pollution in the winter and the identical meteorological conditions on the ground. The impact on the diffusion and the interregional transport of $PM_{2.5}$ were also analyzed. The conceptual schemes of the surface synoptic situation affecting $PM_{2.5}$ pollution were extracted. The results obtained in the study are expected to contribute to the improvement of $PM_{2.5}$ forecasts in two urban agglomerations.

Table 1
The Number of Days With Valid $PM_{2.5}$ Data for Each Month in the Winter During 2013–2019

	Month		
Year	January	February	December
2013	-	-	30
2014	26	21	31
2015	31	28	31
2016	31	28	31
2017	31	28	31
2018	31	28	31
2019	31	28	-

2. Data and Methods

2.1. Ground-Based $PM_{2.5}$ Data

The hourly $PM_{2.5}$ concentrations in the winter from December 2013 to February 2019 were obtained from the China air quality online monitoring and analysis platform (https://quotsoft.net/air/) provided by the Ministry of Environmental Protection of China. It includes nearly 1,500 ambient air quality monitoring stations covering different climatic zones in China (Figure 2). In all these stations, $PM_{2.5}$ concentrations are measured using the Tapered Element Oscillating Microbalance (TEOM, Model RP1400) instruments from Thermo Scientific Company, USA. In the present research work, the daily mean concentrations from all sites are used and selected based on the following criteria: (1) Data with negative or missing values are removed, and (2) the daily mean $PM_{2.5}$ concentration is calculated when more than 20 hours of valid data is available for that day. More details about the observations and data use and processing are provided in Hou et al. (2019). Table 1 lists the number of days for each month with valid $PM_{2.5}$ concentration data during the study period over entire China.

In this study, we focused on the two most populated and polluted regions (BTH and YRD) in China. The mean $PM_{2.5}$ mass concentrations over the BTH (36°–41°N, 113°–119°E) and YRD (28.5°–33°N, 118.5°–123°E) (Figures 1 and 2) areas were obtained from the respective 133 and 135 air quality monitoring sites installed over the regions.

2.2. Meteorological Data

The surface-level wind components, relative humidity, SLP, planetary boundary layer height, pressure, geopotential height, and temperature at the isobaric level were obtained from the Final (FNL) Operational Global Analysis data of the NCEP/NCAR reanalysis (Kalnay et al., 1996) with a horizontal resolution of $1° \times 1°$ in the winter period during 2013–2019. The study domain covers 20°–50°N and 100°–130°E including mainland China, Mongolia, and Siberia. The NCEP/NCAR FNL SLP reanalysis data are available for 00:00, 06:00, 12:00, and 18:00 UTC. In this study, the daily mean of the FNL data is calculated to eliminate disturbances caused by local small-scale systems such as land and sea breezes, and the characteristics are emphatically analyzed.

The precipitation data are used in this study to determine the wet deposition of $PM_{2.5}$ during different circulation types. The gridded hourly precipitation data with a resolution of $0.1° \times 0.1°$ were obtained from the National Meteorological Information Center (http://data.cma.cn/data/cdcdetail/dataCode/SEVP_CLI_CHN_MERGE_CMP_PRE_HOUR_GRID_0.10.html), by combining the ground-based measurements with satellite products. The ground-based observations of precipitation data include the hourly precipitation of more than 30,000 automatic observation stations (including national and regional automatic stations) in China. The satellite precipitation product is obtained from real-time satellite inversion CMORPH precipitation products developed by the climate prediction center of NCEP. The spatial resolution of the original CMORPH data is 8 km, and the time resolution is 30 min.

2.3. Method

In the present work, the obliquely rotated T-mode principal component analysis (T-PCA) method is used to identify the dominant surface wind circulations and SLP types over the study area. This method is proposed to classify the synoptic circulation patterns due to its better performance in terms of its reproduction of predefined types, temporal and spatial stability, and less dependence on preset parameters (Gong & Richman, 1992; Huth, 1996, 2000; Huth et al., 2008; Lyons & Bonell, 1994; White et al., 1991). For this classification, the software was used which was developed within the framework of COST action 733 (http://cost733.geo.uni-augsburg.de/cost733class-1.2) (Huth et al., 2016; Philipp et al., 2014, 2016). A detailed description of the procedure followed in the COST 733 toolbox has been reported by Philipp et al. (2010). The calculation methods of the obliquely rotated T-mode PCA are shown in the supplementary file of Li et al. (2019). The accurate results of the circulation types obtained from the model show that the prevailing weather situation affects the changes in fine PM pollution.

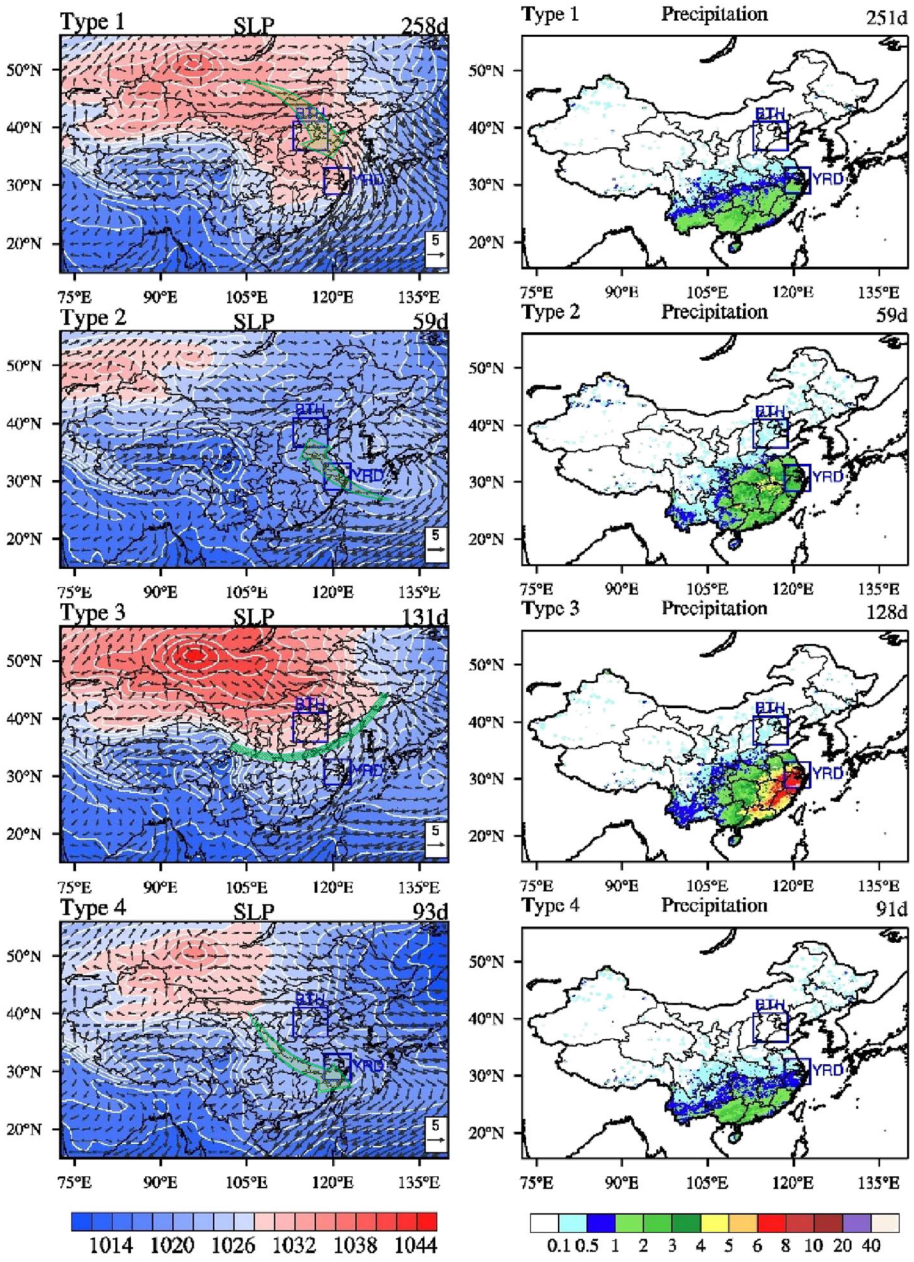

Figure 1. Four different weather patterns of sea level pressure (SLP in hPa) overlaid with the surface wind (unit: m/s) in the winter during December 2013–February 2019 (left column). The right column shows the daily mean cumulative precipitation (mm/day) corresponding to the weather patterns. The number at the top right of each figure indicates the number of days when the corresponding weather type occurred during the 7-year study period. The green arrow is the dominant wind direction, and the green curve in the SLP figure for Type 3 is the approximate position of the front.

Following the air quality standards of China, clean days are defined as days with daily $PM_{2.5}$ less than 75 $\mu g/m^3$ (defined as C or clean); light-polluted days are days with daily $PM_{2.5}$ between 75 and 115 $\mu g/m^3$ (L or light); moderately polluted days are days with daily $PM_{2.5}$ larger than 115 $\mu g/m^3$ and smaller than 150 $\mu g/m^3$ (M or moderate); on heavily polluted days the daily $PM_{2.5}$ is larger than 150 $\mu g/m^3$ (H or heavy). Besides, this study introduces the 24-hour change of $PM_{2.5}$ concentrations, referred to as change rate, to explore the factors that affect the $PM_{2.5}$ accumulation or dissipation rate. The calculation method is

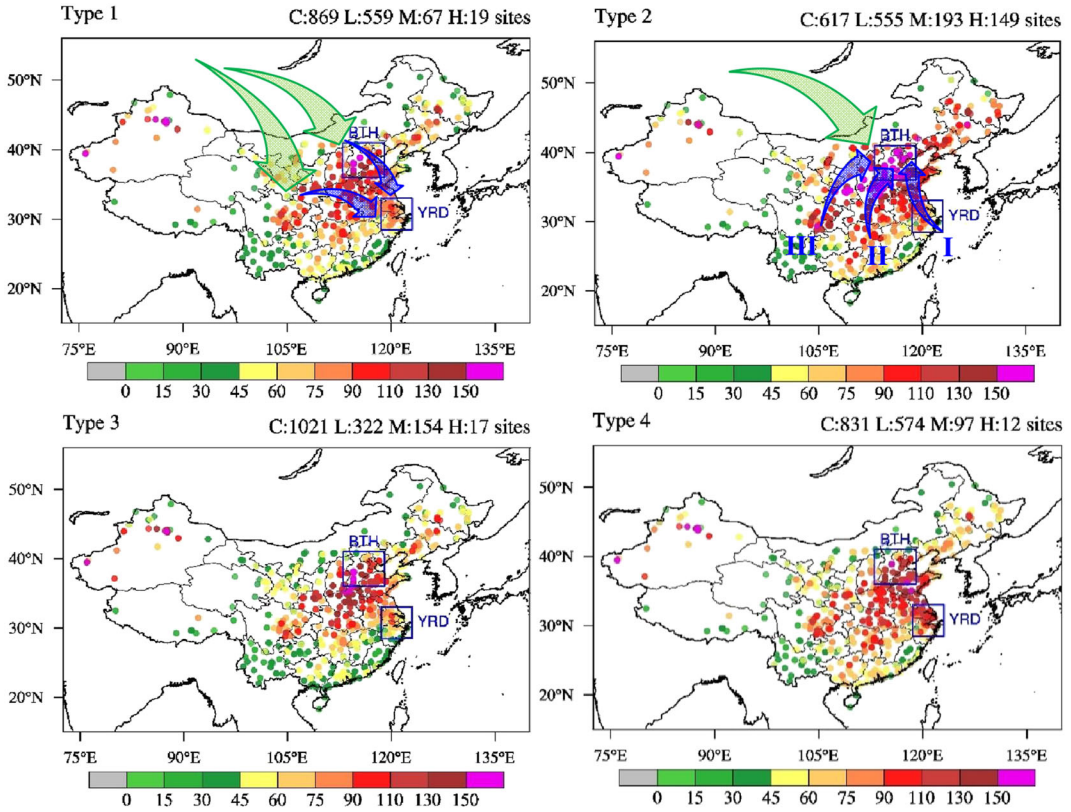

Figure 2. Mean $PM_{2.5}$ concentrations during the four types of synoptic weather situations, color coded as indicated by the color bars at the bottom. The numbers in the upper right indicate the number of sites at different pollution levels (C = clean; L = light; M = moderate; H = high; see text for definitions). The green arrows in the top two figures indicate the southward movement of the Siberian High. The blue arrows show the sample of probable transport pathways to the YRD during Type 1 conditions and to the BTH during Type 2 conditions. The meaning of I, II, and III on these arrows are explained in the text.

$$dPM_{2.5}{}^{t} = PM_{2.5}{}^{t} - PM_{2.5}{}^{t-1}$$

where $PM_{2.5}{}^{t}$ is the daily average concentration of $PM_{2.5}$ on the day (t); $PM_{2.5}{}^{t-1}$ is the daily average concentration of $PM_{2.5}$ on the previous day ($t-1$). $dPM_{2.5}{}^{t} > 0$ implies that $PM_{2.5}$ increased from the previous day (accumulation), and likewise, $dPM_{2.5}{}^{t} < 0$ implies a decrease of $PM_{2.5}$ (dissipation).

Note that it is difficult to exclude the impact of emissions on pollution events in observation, and hence, the study did not consider the impact of the implementation of emission reduction policies in the analysis process. In addition, the implementation of emission reduction measures will highlight the adverse weather factors. The polluted weather may gradually change to clean weather under the situation, which makes our concise pollution conceptual model of pollution more reliable. In our discussion, we also analyzed the process of pollution accumulation using $dPM_{2.5}$. Despite emission reduction, the process of pollution accumulation caused by meteorological factors should remain unchanged.

To reveal the influence of the thermal stability of the boundary layer on pollution, the stable energy of the atmosphere below 900 hPa (about 1 km above the surface) is calculated in this study based on pressure, height above the surface, and temperature from the FNL data. Stable energy is a parameter proposed by Shang et al. (2001) to describe the stability of the atmospheric layer from the surface to a specific height, that is, low-level stable energy. This method has been used over the Lanzhou (Shang et al., 2001), BTH (Yang et al., 2017), and Pearl River Delta (PRD) (Wu et al., 2019) regions. The equations used to calculate the stable energy are described in detail by Shang et al. (2001).

3. Synoptic Classification and Corresponding $PM_{2.5}$ Distribution

Based on the T-PCA and the explained cluster variance (Hoffmann & HeinkeSchlüNzen, 2013; Ning et al., 2019; Philipp et al., 2014) methods, four different types of meteorological situations were selected. For each of the four types of weather situations, the SLP and wind components over the study area were calculated with the COST 733 toolbox. The SLP patterns overlaid with the wind fields are shown in Figure 1 (left column), together with the cumulative precipitation (right column). Figure 1 shows the apparent differences in the core pressure distributions for the four types of weather conditions. The region covered by high pressure and average latitude and longitude of the Siberian High winds (Table S1) is also different for the four types of situations. These four types of weather conditions are highly representative and suitable for our study.

The Type 1 weather pattern is most common and occurred on 258 days during the 7-year study period. Most of eastern China experienced the East Asian winter monsoon induced by the Siberian High winds, which can be seen in Figures 1 and S2. The boundary of the 1,028 hPa isobaric line reached as far south as ~25°N in China. Therefore, the westerly winds prevailed over the BTH and northerly winds in the YRD area. A weak rain belt occurred to the south of the Siberian High, and the rain area is concentrated in southern China. The Type 2 situation was observed for 59 days. During this weather pattern, a weak Siberian High was situated in over northwestern China. At 850 hPa (Figure S2), an anomalous western North Pacific subtropical high was located over the East China Sea which weakened the strength of the winter monsoon (He et al., 2019; Wang et al., 2010; Wang & Chen, 2010). In this situation, the pressure differences over the BTH and YRD areas were relatively small and, thus, also the wind speed. This weather situation was not conducive to the diffusion and dilution of pollutants which matches the results of Zhang et al. (2012) and Miao et al. (2017). Besides, the weak southerly winds in the BTH might result in the transport of pollutants from central and southern China to the north, thereby aggravating the pollution in the BTH region. However, there was some weak precipitation to the south of the BTH, which may have resulted in wet removal of particles. During the Type 3 weather pattern (Figure 1), which occurred during 131 days, the cold Siberian High was intense and moving south, which affects the northern areas of China (BTH, Shandong Peninsula). The front was close to the YRD which resulted in much precipitation in that area. The western North Pacific subtropical high was weak (Figure S2). During Type 4 (93 days), the Siberian High was weak, and there was a low-pressure area in the East of China. The low pressure was a profound system (Figure S2), named the Northeast Cold Vortex. Blocked by this low-pressure system, the cold air moved slowly southward along the eastern side of the Tibetan Plateau. The pressure differences in the East of China were small, especially over the YRD, which is conducive to the accumulation of pollutants. During this weather type, the rain belt was mostly in the south, and the precipitation was weak.

The $PM_{2.5}$ concentrations at the ground-based stations, averaged over the 7-year observation period for each type of weather situation, are presented in Figure 2. At the top of each plot in Figure 2 is indicated with how many stations experience clean, light, moderate, and high $PM_{2.5}$ concentrations. The maps show the spatial distribution of the $PM_{2.5}$ levels across China for the four types of weather conditions. The number of clean sites (C) was most significant during Type 3, with 1,021 sites. Thus, most of the sites in China experienced relatively low $PM_{2.5}$ concentrations, which is related to intense precipitation and wet removal. During Types 1 and 4 weather conditions, the number of clean sites was similar (869 and 831, respectively). The number of moderately polluted sites during Type 1 was the lowest (67). The number of severely polluted sites was smallest during Type 4 (12). However, the largest number of highly polluted sites was observed during Type 2 weather conditions, with 149 stations, and they are concentrated in the BTH and surrounding areas. This is mainly related to the relatively stable weather and interregional transport under the influence of the weak eastern high pressure.

The southward movement of Siberian High has three paths: the east, the middle, and the west. Based on the pathways of the cold air movement and the distribution of the surface $PM_{2.5}$ concentrations, we speculate that there may be two effective pathways to transport pollutants to the YRD (see the blue arrows in Figure 2 Type 1). One is from the BTH and Shandong to the YRD, and the other one is from the Henan, Hubei, and Anhui provinces in central China to the YRD. Besides, there were three high-concentration bands of $PM_{2.5}$, especially during Type 2 (see the blue arrows in Figure 2 Type 2), which are connected to the YRD (I), the Two Lakes area (II), and the Sichuan Basin (III). When the pollutants are transported to

the BTH along with one of these three pathways, the pollution in the BTH may be significantly aggravated. The regions between the YRD, the Lakes area, and the BTH are mostly plain areas. Once the southerly wind prevails on a large scale, it is very possible to transport pollution to the BTH over a long distance. However, Sichuan is located in a basin, and there are many mountains between BTH and Sichuan, such as the Daba and Hua mountain ranges, rendering difficult for the transport of pollutants.

4. Synoptic Patterns and $PM_{2.5}$ Pollution Over the BTH Region

4.1. Differences in Weather Types During Different Pollution Levels

Figure 3a shows the average $PM_{2.5}$ concentrations and the frequency of occurrence of varying pollution levels over the BTH, together with the precipitation. The lowest $PM_{2.5}$ concentrations (94.8 $\mu g/m^3$) and the rate of occurrence of pollution (47.6%) occurred during Type 1 meteorological conditions. The $PM_{2.5}$ levels and the frequencies of occurrence of pollution and severe pollution days were the highest during Type 2 meteorological conditions with 153.3 $\mu g/m^3$, 90.7% and 40.7%, respectively. The average precipitation in the BTH was the highest during Type 2 meteorological conditions, about 0.15 mm/day. The simultaneous occurrence of the highest $PM_{2.5}$ concentrations and the highest precipitation rate implies that wet deposition is not an essential factor for the removal of the aerosol particles in this case of accumulation during low wind conditions. This means that the influence of the eastern weak high pressure is most prone to severe pollution events in the BTH.

Figure 3b shows the average 24-hour $PM_{2.5}$ change rate (box) and the distribution of the number of days with a specific change rate (tower). From these data, it is evident that during Type 1 meteorological conditions $PM_{2.5}$ accumulated with an average rate of 6.2 $\mu g/(m^3 \cdot day)$, even though the number of accumulation days (154) was much higher than the number of dissipation days (82) (Figures S3b and S3c). As shown in Figure 3b, there were many accumulation days, but on most of them, the accumulation rate was low. Therefore, Type 1 is a type of weather with a slow accumulation of pollution. During Type 2 meteorological conditions, the $PM_{2.5}$ accumulation rate was high with an average of about 28.7 $\mu g/(m^3 \cdot day)$. The number of accumulation and dissipation days was 41 and 11, respectively (Figures S3b and S3c), with a high rate on most of the accumulation days (Figure 3b tower). Therefore, Type 2 is a type of weather with a rapid accumulation of pollution. Type 3 meteorological conditions are conducive to $PM_{2.5}$ dissipation, with the fastest average rate of about -23.4 $\mu g/(m^3 \cdot day)$. $PM_{2.5}$ accumulated during only 43 days, and dissipation occurred during the remaining 75 days. It is a fast-dissipating weather type. During Type 4 meteorological conditions, $PM_{2.5}$ accumulated during 34 days and dissipated during 45 days; the average rate was -3.1 $\mu g/(m^3 \cdot day)$. It is a slow-dissipating weather type.

The above analysis shows that, although the rate of accumulation of pollution in Type 1 weather condition is not high, the number of days is large, so the effect of Type 1 meteorological conditions on the total pollution is considerable. Figure S3a shows that there were 121 BTH pollution days during Type 1 meteorological conditions for the 7-year study period, which is much higher than for other weather types. Therefore, it is crucial to determine the differences between pollution and clean days during Type 1 meteorological conditions. To this end, the mean SLP and surface wind distributions for clean, light, moderate, and high $PM_{2.5}$ concentrations during Type 1 meteorological conditions over BTH are plotted in Figure 4.

It is evident from Figures 4 and S4 in the supporting information that there are significant differences in the SLP and surface winds during clean and polluted days (see the green [clean] and gray [polluted] arrows in Figure 4) and in the geopotential height and wind field at 850 and 500 hPa. During the clean days, the atmospheric pressure in the Siberian High was higher than during the polluted days while the low pressure in northeast China was lower (both at 850 and 500 hPa in Figure S4). The wind speed in the BTH area was elevated from northerly directions, which is conducive to the diffusion and dilution of pollution. During the polluted days, the atmospheric pressure in the BTH region was weaker (about 1,030 hPa); the northerly wind was weak and turned to southerly directions during 36% of the time (Table 2). During moderately and severely polluted days, the pressure in the eastern region was abnormally high, and the wind speed in the south was high. At 850 and 500 hPa (Figure S4), there were anomalous southerly winds over the BTH associated with the weakened winter monsoon. Therefore, the frequency of southerly winds provides a strong indication of pollution in the BTH region, in good agreement with the results of He et al. (2019). Also,

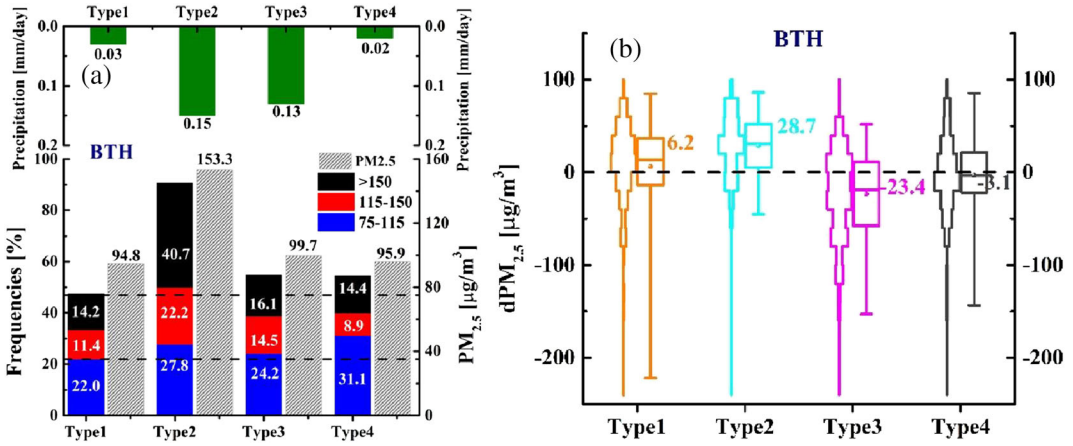

Figure 3. (a) Average $PM_{2.5}$ concentrations (gray primary columns), frequency of occurrence of $PM_{2.5}$ pollution level (colored columns) and precipitation (green columns), and (b) the average 24-hour $PM_{2.5}$ change rate (box, g/(m^3·day; mean values are indicated) and the distribution of the number of days with a specific change rate (tower) for the four types of meteorological conditions in the BTH region; 75–115 μg/m^3 is light fine particle pollution; 115–150 μg/m^3 is moderately fine particle pollution; >150 μg/m^3 is heavy fine particle pollution. The two dotted lines represent the $PM_{2.5}$ values of 35 and 75 μg/m^3, respectively. The width of the tower represents the number of days.

given the prevailing wind direction, there is likely a transport process from the YRD to BTH, namely, along the path I shown in Figure 2. Table 2 shows that the average stable energy was only 167.9 J/cm^2. But the frequency of southerly winds was relatively high during polluted days, and the accumulation speed ($dPM_{2.5}$) was positive. Hence, the pollution during Type 1 meteorological conditions is likely caused by the transport of pollutants along the path I.

During Type 2 meteorological conditions, the location of the weak eastern high pressure is westward during clean days, leading to westerly winds in the BTH and its southern regions (Figure S5). Westerly winds cause

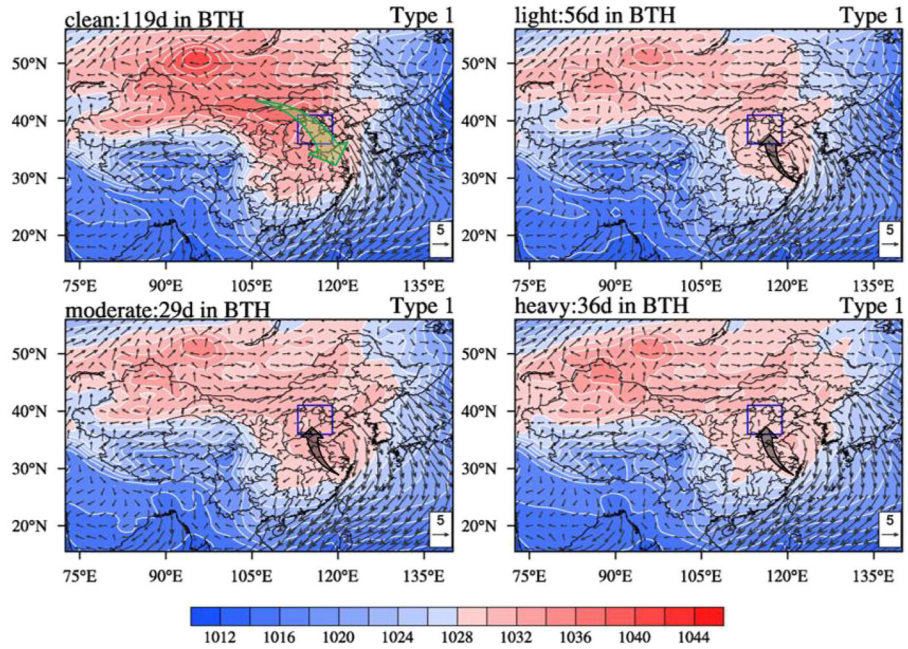

Figure 4. The distribution of the mean sea level pressure (SLP) and surface winds during Type 1 meteorological conditions over the BTH region (indicated with the blue box) with clean, light, moderate, and high $PM_{2.5}$ concentrations. The green arrow shows the dominant wind direction, and the dark gray arrows indicate the actual surface winds in the region.

Table 2
Meteorological Parameters During Each of the Four Weather Types in the BTH Area for Different Pollution Levels

		$PM_{2.5}$ μg/m^3	$dPM_{2.5}$ μg/(m^3·day)	Prec mm/day	RH %	Speed m/s	wind_dir[a] %	PBLH m	E_stab J/cm^2
Type 1	Mean	94.8	6.2	0.03	40.7	2.4	31.1	350.7	167.9
	C	48.3	−13.6	0.03	35.1	2.9	21.9	452.9	137.8
	L	103.4	22.0	0.02	42.1	2.2	36.4	279.6	185.4
	M	140.3	27.5	0.02	46.8	2.0	42.0	249.0	191.2
	H	204.1	34.7	0.02	53.2	1.9	44.2	222.8	223.3
Type 2	Mean	153.3	28.7	0.15	53.2	2.1	36.9	246.3	239.8
	C	67.0	19.1	0.30	46.3	2.2	54.8	295.8	189.4
	L	109.1	18.3	0.23	48.2	2.0	30.3	295.3	207.9
	M	139.0	23.2	0.17	52.1	2.3	30.0	242.3	252.0
	H	210.9	41.3	0.03	58.4	1.9	40.4	193.8	249.7
Type 3	Mean	99.7	−23.4	0.13	49.1	2.7	9.3	405.1	165.4
	C	50.6	−41.1	0.06	44.1	3.2	5.3	523.6	135.6
	L	95.7	−7.0	0.04	48.3	2.5	11.8	357.3	168.0
	M	136.7	−14.7	0.36	55.3	2.4	12.7	283.2	208.8
	H	202.3	−9.3	0.15	57.7	2.1	13.5	279.0	207.6
Type 4	Mean	95.9	−3.1	0.02	40.3	3.0	28.1	417.9	177.3
	C	50.4	−13.9	0.02	36.7	3.5	23.5	543.1	140.9
	L	99.9	−3.7	0.03	40.5	2.8	26.6	384.4	181.5
	M	141.1	30.5	0.01	44.8	2.3	43.2	271.4	194.6
	H	189.2	15.7	0.01	46.0	2.5	35.3	244.3	243.5

[a]*Note*. Percentage of wind directions having a southerly component (90°–180°).

relatively high fractions of southerly wind components during the clean period as shown in Table 2. During severely polluted days, the location of the weak eastern high pressure was in the south where the intensity is vigorous, leading to southerly winds in the BTH and further south, which are conducive to the transport of pollution from the south to the north. The relatively high humidity, low wind speed, low PBL, and high stability energy during Type 2 meteorological conditions (Table 2) indicate that the atmosphere in the BTH region was stably stratified. During all four pollution levels, $PM_{2.5}$ accumulated ($dPM_{2.5} > 0$), and the average accumulation speed reached 41.3 μg/(m^3·day) during severely polluted days. Also, the average fraction of southerly wind components was high. Weak southerly airflow transported pollutants from the south to the BTH, which ultimately resulted in the worst pollution during Type 2. The high pollution in the BTH during Type 2 meteorological condition is the combined result of local accumulation and slow advection of pollutants from elsewhere.

During Type 3 meteorological conditions, the BTH was mostly sunny with fine weather after the front (Figure S6), and $PM_{2.5}$ was in a dissipative state (Table 2). In general, it is clear that heavier the pollution, the slower the diffusion rate. During Type 4 meteorological conditions, the average wind speed and the boundary layer height were high, which promotes the dissipation of pollution. But the dissipation only occurred during clean and lightly polluted days. During moderate and severe pollution days, when the location of the northeast cold vortex was to the west, the southerly wind transported air from the two lakes to the BTH (Figure S7), causing the transport of pollutants along path II in Figure 2. At this time, the frequency of southerly winds in the BTH increased to more than 35%, and $PM_{2.5}$ turned into a rapid accumulation state. Therefore, the moderate and severe pollution days during Type 4 are likely due to transport along path II.

4.2. Establishment of Clean and Polluted Weather Conceptual Models

Based on the above analysis, conceptual weather models in the BTH emerge with characteristics as shown in Figure 5. The left column panels show the clean weather models for pollution dissipation, and the right column panels indicate the conceptual weather models for pollution accumulation. The clean weather models conducive to pollution dissipation are divided into three types: the southward movement of strong cold air during Type 1 meteorological conditions, the fine weather after front during Type 3, and the intense pressure gradient between the strong Siberian high and the northeast cold vortex during Type 4. The unfavorable weather models conducive of pollution accumulation have common characteristics, that is, the

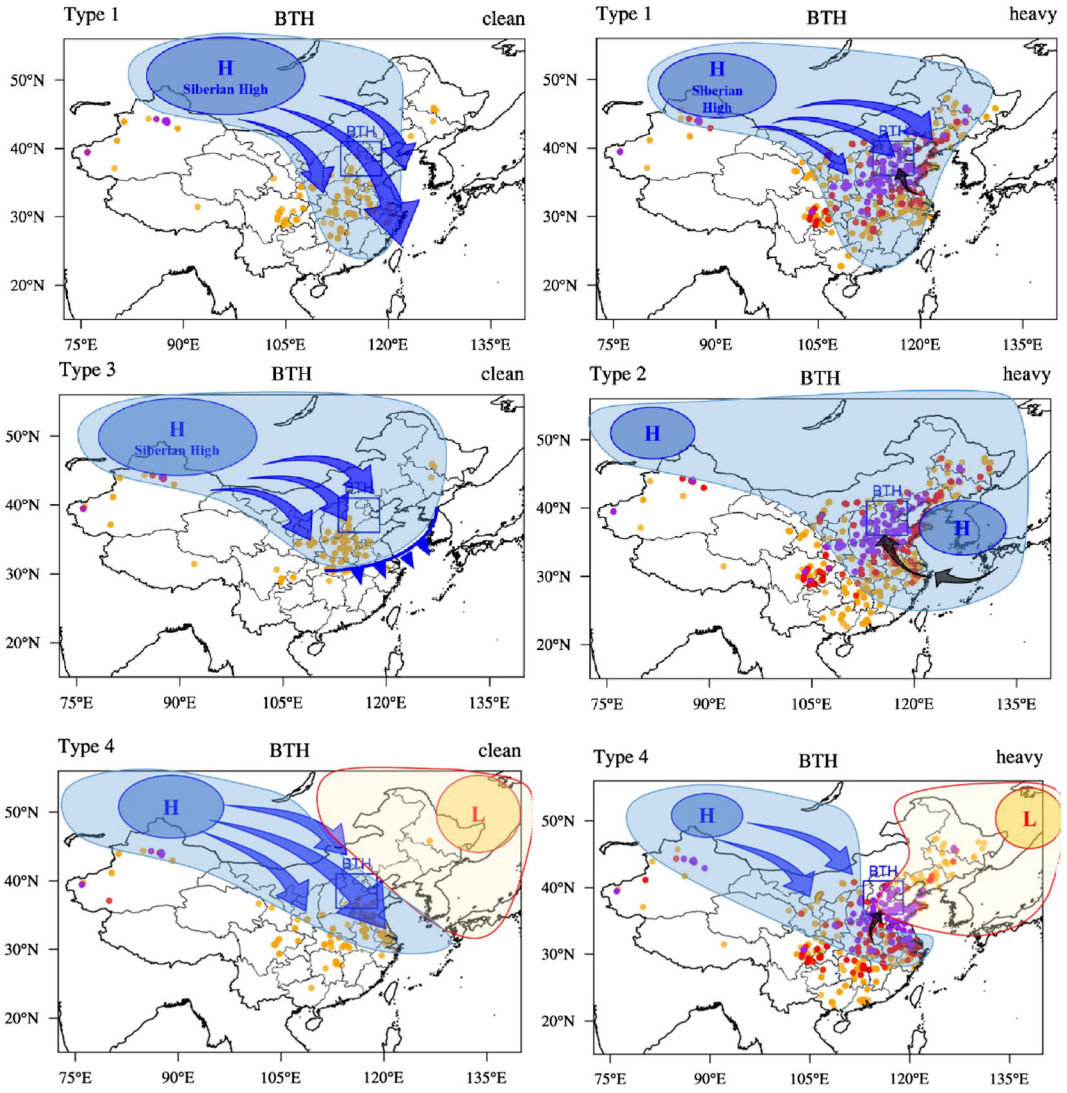

Figure 5. Conceptual models during four meteorological conditions over the BTH region. The left column panels correspond to the models leading to clean air, and the right column panels indicate the models conducive to the formation of pollution.

occurrence of southerly winds, and can be classified into three categories: weak Siberian High and slow southward movement of cold air during Type 1, weak eastern high pressure during Type 2, and southward flow of cold air along the east of the Tibetan Plateau (named west path) during Type 4. There are two transport routes of pollutants to the BTH: one from the YRD and Shandong to the BTH, mainly during Types 1 and 2 meteorological conditions; the other one from the Hubei and Henan provinces to the BTH, mostly during Type 4 meteorological conditions. Therefore, considering the transport with unfavorable weather conditions during Types 1 and 2 meteorological situations, the reduction of local emissions and in the YRD and Shandong is a feasible method to reduce the air pollution in the BTH while the reduction of local emissions and in Hubei and Henan may be beneficial for the improvement of air quality in the BTH area during Type 4 meteorological conditions.

5. Synoptic Patterns and $PM_{2.5}$ Pollutions Over the YRD Region

5.1. Differences in Meteorological Conditions During Different Pollution Levels

The average $PM_{2.5}$ concentrations and the frequency of occurrence of different pollution levels over the YRD during the four meteorological situations are presented in Figure 6a, together with the precipitation. The

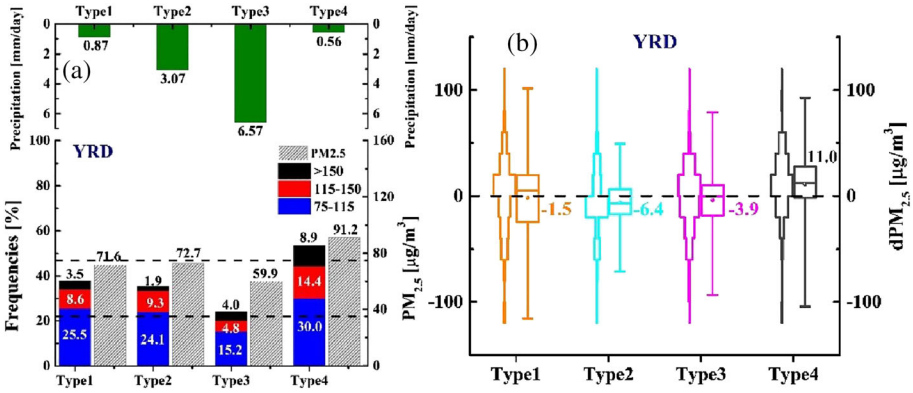

Figure 6. Same as Figure 3 but for the YRD.

average 24-hour $PM_{2.5}$ change rate and the distribution of the number of days with a specific change rate are shown in Figure 6b. The meteorological parameters for the YRD study are collected in Table 3. The average $PM_{2.5}$ concentrations and the frequency of occurrence of polluted days were the lowest during Type 3 meteorological conditions, with 59.9 μg/m^3 and 24.0%, respectively. These low values are partly attributed to the heavy precipitation with 6.57 mm/day. During Type 4, the average $PM_{2.5}$ concentrations and the occurrence of pollution days over the YRD were the highest, with 91.2 μg/m^3 and 53.3%, respectively. The average 24-hour $PM_{2.5}$ change rate (box in Figure 6b) shows that $PM_{2.5}$ was dissipated during Types 1–3. The average dissipation rate was fastest during Type 2 conditions with −6.4 μg/(m^3·day). During Type 4 meteorological conditions, the average accumulation speed was high (11.0 μg/[m^3·day]). The distribution of the number of days with a specific change rate (tower) shows that the number of days with $dPM_{2.5} > 0$ was large during Type 1 meteorological conditions, and was concentrated in the low accumulation speed (Figure 6b). The accumulation of pollution during this weather situation was quite slow, and the negative average rate indicates that it dissipated faster than that it accumulated. Also, the number of polluted days during Type 1 was more significant, with 96 days (Figure S8a) than during other weather types. The number of severely polluted days was also the highest, and most of them were accumulating. Therefore, we focused on the weather difference corresponding to different pollution levels during Type 1.

Figure 7 shows the distribution of SLP and surface winds for Type 1 meteorological conditions over the study area for clean, light, moderate, and heavy pollution in the YRD. As shown in Figure 2, the $PM_{2.5}$ concentrations were high in the central and northern parts of China upwind of the YRD. Hence, during westerly winds, pollution was transported to the YRD. Besides, there may be regional transport of pollution, which intensifies the $PM_{2.5}$ pollutions in the YRD region. Therefore, the westerly wind frequency is highly indicative of pollution in the YRD. During Type 1 meteorological conditions, the dominant wind direction during the polluted days over the YRD was from the northwest. Figure 7 shows the severely polluted days that occurred when the Siberian High is very strong with an atmospheric pressure of 1,043 hPa and influenced an extensive area. However, the cold air traveled towards the southwest, and strong northwest winds prevail in the YRD. This results in an average wind speed of 4.3 m/s, and the frequency of westerly winds reached maximum values of up to 76.4%, and the accumulation rate of $PM_{2.5}$ increased to 31.5 μg/(m^3·day) (Table 3). The height of the boundary layer did not decrease substantially concerning clean days, and the stability energy of the bottom layer was not high, which further illustrates the contribution of transport to pollution episodes, which is consistent with the results of Kang et al. (2019). Also, considering the prevailing wind direction, the light and moderate pollution in the YRD area may be affected by transport from the BTH and Shandong, and the heavy pollution may be affected by transport along the two pathways shown in Figure 2a. In general, the pollution in the YRD during Type 1 meteorological conditions is significantly influenced by transport from northern and central China.

During Types 2–4 meteorological conditions, there were fewer days of heavy pollution, in particular during Type 2 when there was only 1 day with heavy pollution, which is not statistically significant. Therefore, heavy and moderate pollution were combined in the analysis. The frequency of the westerly wind is found low during Type 2, with the lowest boundary layer height, high stable energy, and a relatively calm

Table 3
Meteorological Parameters During Each of the Four Weather Types in the YRD Area for Different Pollution Levels

		$PM_{2.5}$ μg/m^3	$dPM_{2.5}$ μg/(m^3·day)	Prec mm/day	RH %	Speed m/s	wind_dir[a] %	PBLH m	E_stab J/cm^2
Type 1	Mean	71.6	−1.5	0.87	63.9	4.3	44.7	693.1	155.5
	C	48.4	−13.0	1.09	63.5	4.6	40.7	738.4	148.9
	L	92.0	9.9	0.67	63.7	3.8	47.9	625.0	164.8
	M	131.0	29.0	0.32	66.1	3.7	56.7	559.5	191.9
	H	172.5	31.5	0.44	63.0	4.3	76.4	680.2	143.1
Type 2	Mean	72.7	−6.4	3.07	74.9	3.1	8.7	353.3	305.9
	C	49.4	−10.3	4.10	76.5	3.3	5.8	378.7	304.2
	L	91.4	−3.5	3.33	70.4	2.8	9.8	356.8	298.9
	M&H	203.3	−11.8	0.10	71.7	2.4	8.4	302.7	278.2
Type 3	Mean	59.9	−3.9	6.57	80.4	4.3	27.6	520.5	243.6
	C	41.3	−8.4	7.73	82.5	4.7	23.7	551.8	244.4
	L	91.6	9.3	2.43	71.3	3.2	42.7	474.6	218.0
	M&H	134.0	8.3	4.82	81.6	3.2	29.3	337.1	316.1
Type 4	Mean	91.2	11.0	0.56	62.5	3.3	33.8	496.2	214.2
	C	52.6	3.6	0.89	63.3	3.6	36.9	534.8	213.2
	L	98.4	16.9	0.33	60.2	3.4	33.6	486.8	194.1
	M&H	212.0	36.9	0.20	64.9	2.5	39.0	429.9	231.7

[a]*Note*. Percentage of wind directions having a westerly component (180°–360°).

atmosphere. However, during Type 2 conditions pollution dissipated, which means the more onerous the pollution, the faster the dissipation rate, which is related to the clean east wind (Figure S9). Thus, Type 2 is a fast-dissipating meteorological condition cleared by the east wind. During Type 3 meteorological conditions, there was a large amount of precipitation (Table 3). During the clean period, the precipitation

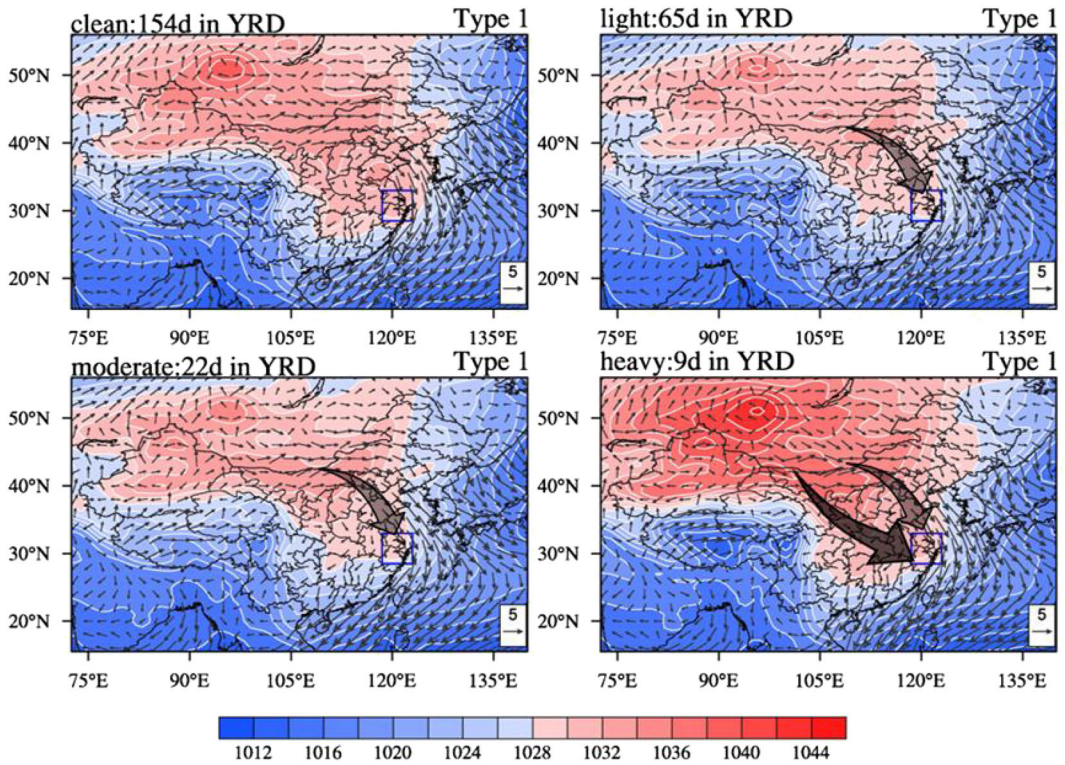

Figure 7. Spatial distributions of the mean sea level pressure (SLP) and surface winds during Type 1 meteorological conditions over the YRD region (indicated with the blue box) for clean, light, moderate, and high $PM_{2.5}$ concentrations. The black arrows in the figure show the large-scale dominant wind direction.

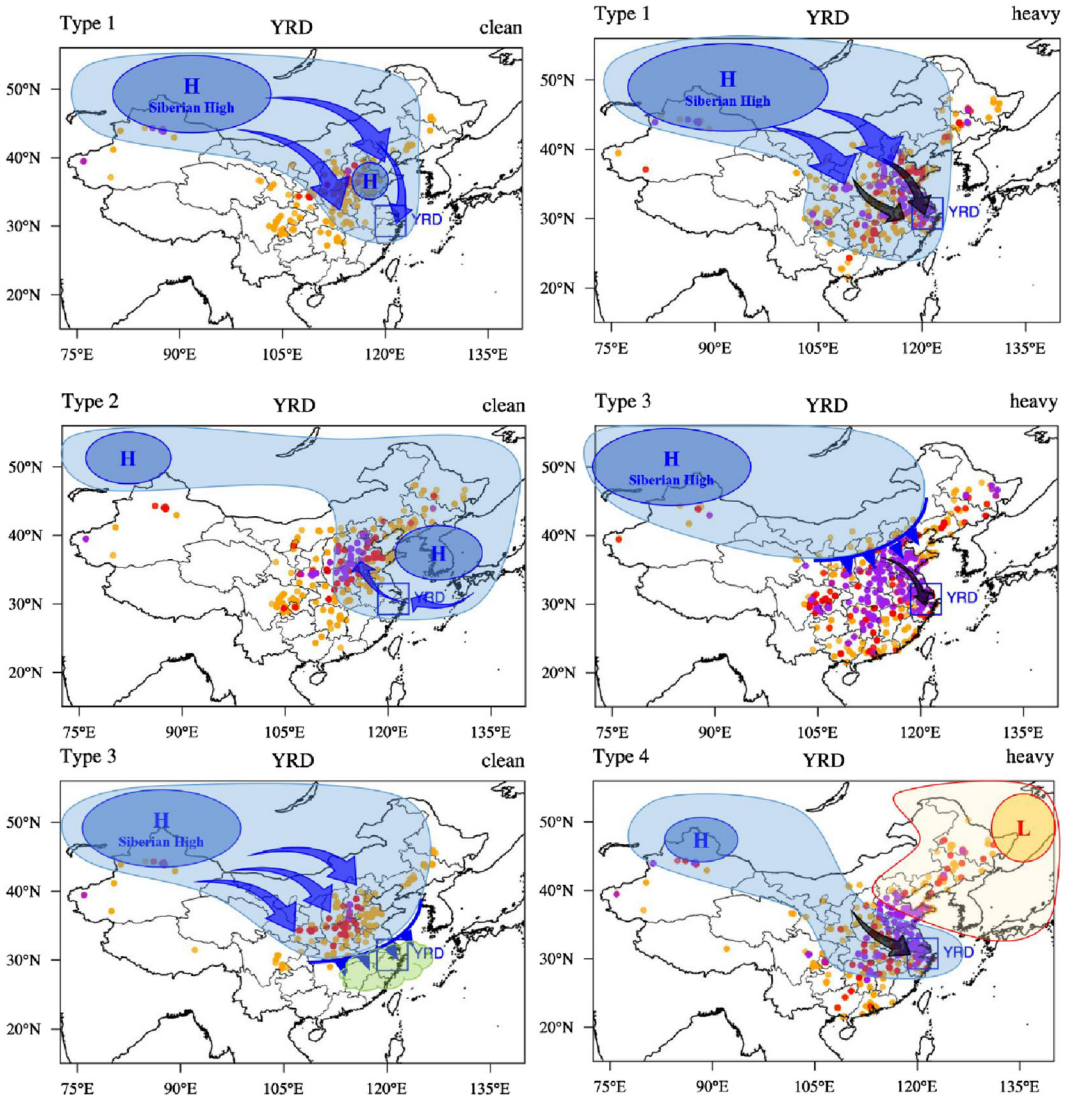

Figure 8. Same as in Figure 5 but in the YRD area.

reached 7.73 mm/day, and the effect of wet removal is apparent. During the polluted period, the intensity of the Siberian High was weak (~1,042 hPa), and the range is small (Figure S10). The southeast boundary of the 1,028 hPa isobaric line was located near the BTH area. The weak precipitation, with the strong westerly wind, low boundary layer height, and increased stable energy, led to a slow accumulation of $PM_{2.5}$ (Table 3). Generally, Type 3 conditions lead to dissipative weather with removal by wet deposition. In Type 4, the cold air moves southward along the eastern side of the Tibetan Plateau, and there will be a transport of pollution from Anhui province and other regions in the west to the YRD region (Figure S11). Hence, the atmosphere in the YRD was relatively stable, with less precipitation. Thus, during Type 4 meteorological conditions the weather is calm with the fast accumulation of $PM_{2.5}$.

5.2. Establishment of Conceptual Weather Models Describing Pollution in the YRD

Based on the above analysis, conceptual weather models in the YRD emerge with characteristics as shown in Figure 8. The panels in the left column show the weather models leading to the dissipation of pollution; the panels in the right column present the weather models leading to the accumulation of pollution. The weather models for pollution dissipation are divided into three types: the southward movement of strong cold air with a weak high pressure in Shandong during Type 1, easterly wind at the bottom of weak

eastern high-pressure during Type 2, and a situation with frontal activity with intense precipitation and high wind during Type 3. The weather models promoting the accumulation of pollution can also be classified into three types: slow southward movement of a weak Siberian High (light and moderate pollution) and southward movement of a strong Siberian High along two paths (heavy pollution) during Type 1, northerly front of weak Siberian High during Type 3, and southward movement of cold air along the east of the Tibetan Plateau (named west path) during Type 4. There are two primary transport routes of pollutants to the YRD: one from the BTH and Shandong to the YRD mainly during Types 1 and 3 meteorological conditions and the other from Hubei and Anhui provinces to the YRD during Types 1 and 4 meteorological conditions. Considering the transport during Types 1, 3, and 4, reduction of local emissions and in the BTH, Shandong, Hubei, and Anhui is a feasible method to reduce the air pollution in the YRD.

6. Conclusions

Fine particulate pollution still occurs frequently in some areas of China, especially in the BTH and the YRD. Understanding the meteorological conditions leading to fine particle pollution in these two major urban agglomerations provides crucial guiding significance for forecasting and early warning of pollution events. The characteristics of meteorological conditions and local weather elements during clean and polluted days were analyzed by application of the oblique PCA method with the COST733 toolbox and the concept of daily $PM_{2.5}$ accumulation rates to long-term observations of $PM_{2.5}$, together with precipitation, SLP, and wind field data. Further, conceptual models of pollution dissipation and accumulation conditions during different meteorological situations were evaluated. It should be mentioned that the variability of the emission rate due to the implementation of emission mitigation strategies is not excluded. The main conclusions are summarized as follows.

Four types of meteorological situations were selected based on the differences observed in the spatial distributions of SLP and surface wind speeds. These four types of cases are significantly different and highly representative of the situation in the study area with the occurrence of $PM_{2.5}$. During the most common Type 1 meteorological situation, the Siberian High reaches as far south as ~25°N. Northerly winds prevail, which may be conducive to the transport of pollutants from north to south. During Type 2 conditions, a weak high pressure is situated in the eastern part of China with the widest range of severe pollution, concentrated in the BTH area with the fastest accumulation of pollutants. During Type 3, the Siberian High affects the northern part of China while its associated front causes a large amount of precipitation in the south. In this situation, there is little pollution in most areas in eastern China, and also in the BTH and YRD regions, the pollution dissipates. During Type 4, the weak Siberian High is blocked by the northeast cold vortex and moves towards the south along the southeast side of the Tibet Plateau. It is most likely to cause pollution incidents which accumulate in the YRD area.

Over the BTH, the movement of strong cold air towards the south during Type 1 meteorological conditions, the fine weather behind the front during Type 3 conditions, and the intense pressure gradient between the strong Siberian High and the northeast cold vortex during Type 4 induce the dissipation of pollution in the BTH, resulting in clean days. The frequency of southerly winds provides a high indication of pollution. The weak Siberian High and slow southward movement of cold air during Type 1 conditions, the weak eastern high pressure during Type 2, and the southward movement of cold air along the east of the Tibetan Plateau during Type 4 cause southerly winds in the BTH, which is conducive to the transport of pollution from the south to the north and exacerbates the pollution in the BTH.

Over the YRD, the southward movement of strong cold air with a weak high pressure in Shandong during Type 1, easterly wind removal at the bottom of a weak eastern high-pressure during Type 2, and strong precipitation and windy frontal weather during Type 3 result in the dissipation of pollution in the YRD and thus clean days. The frequency of westerly winds provides a strong indication of pollution in the YRD area. The southward movement of a strong Siberian High along two pathways leads to heavy pollution in the region during Type 1 meteorological conditions. The north front of the weak Siberian High during Type 3 and southward movement of cold air along the east of Tibetan Plateau during Type 4 make the weather in the YRD stable. Therefore, improving air quality requires regional synergy. Emission control measures can be applied along the transport pathways when dominant circulation patterns are predicted.

Conflict of Interest

The authors declare no conflict of interest.

Data Availability Statement

We acknowledge the Ministry of Environmental Protection of China and the China air quality online monitoring and analysis platform (https://quotsoft.net/air/) for providing $PM_{2.5}$ data, the National Meteorological Information Center (http://data.cma.cn/data/cdcdetail/dataCode/SEVP_CLI_CHN_MERGE_CMP_PRE_HOUR_GRID_0.10.html) for providing gridded hourly precipitation data, and the NCEP/NCAR (http://rda.ucar.edu/datasets/ds083.2/) for providing meteorological data.

Acknowledgments

This study was supported by the National Key Research and Development Program of China (Grant No: 2016YFA0602003), the National Natural Science Foundation of China (Grant Nos: 91544229, 41605096, 41605091, and 41805120), and Department of Science and Technology (DST), Science and Engineering Research Board (SERB) sponsored Start-up Research Grant scheme under Science and engineering research board (SERB) of Department of science and technology (DST) (File no. SRG/2020/001445). One of the authors KRK is grateful to the DST, Government of India for the award of the DST-FIST Level-1 (SR/FST/PS-1/2018/35) scheme to the Department of Physics, KLEF. The authors would like to acknowledge Prof. Ping Yang, Editor of the Journal, and the three anonymous reviewers for their helpful comments and constructive suggestions towards the improvement of earlier versions of the manuscript.

References

Anderson, A., Deng, J. J., Du, K., Yan, C. Q., Zheng, M., Sköld, M., & Gustafsson, O. (2015). Regionally-varying combustion sources of the January 2013 severe haze events over eastern China. *Environmental Science & Technology*, *49*, 2038–2043. https://doi.org/10.1021/es503855e

Bei, N. F., Li, G. H., Huang, R. J., Cao, J. J., Meng, N., Feng, T., et al. (2016). Typical synoptic situations and their impacts on the wintertime air pollution in the Guanzhong basin, China. *Atmospheric Chemistry and Physics*, *16*, 7373–7387. https://doi.org/10.5194/acp-16-7373-2016

Bei, N. F., Li, X. P., Tie, X. X., Zhao, L. N., Wu, J. R., Li, X., et al. (2020). Impact of synoptic patterns and meteorological elements on the wintertime haze in the Beijing-Tianjin-Hebei region, China from 2013 to 2017. *Science of the Total Environment*, *704*, 12. https://doi.org/10.1016/j.scitotenv.2019.135210

Cheng, Z., Chen, C. H., Huang, C., Huang, H. Y., Li, L., & Wang, H. L. (2011). Trans-boundary primary air pollution between cities in the Yangtze River Delta. *Acta Scientiae Circumstantiae*, *31*(4), 686–694.

Comrie, A. C., & Yarnal, B. (1992). Relationships between synoptic-scale atmospheric circulation and ozone concentrations in metropolitan Pittsburgh, Pennsylvania. *Atmospheric Environment*, *26*, 301–312. https://doi.org/10.1016/0957-1272(92)90006-E

Dang, R., & Liao, H. (2019). Severe winter haze days in the Beijing–Tianjin–Hebei region from 1985 to 2017 and the roles of anthropogenic emissions and meteorology. *Atmospheric Chemistry and Physics*, *19*(16), 10,801–10,816. https://doi.org/10.5194/acp-19-10801-2019

El-Kadi, A. K. A., & Smithson, P. A. (1992). Atmospheric classifications and synoptic climatology, Prog. *Physical Geography*, *16*, 432–455. https://doi.org/10.1177/030913339201600403

Feng, Y., Wang, A., Wu, D., & Xu, X. (2007). The influence of tropical cyclone Melor on PM_{10} concentrations during an aerosol episode over the Pearl River Delta region of China: Numerical modeling versus observational analysis. *Atmospheric Environment*, *41*(21), 4349–4365. https://doi.org/10.1016/j.atmosenv.2007.01.055

Gong, X. F., & Richman, M. B. (1992). A study of statistical experiment for the application of principal component analysis to regional climate patterns. *Scientia Atmospherica Sinica (in Chinese)*, *16*(6), 649–658.

Guo, J., Lou, M., Miao, Y., Wang, Y., Zhao, Z., Liu, H., et al. (2017). Trans-Pacific transport of dust aerosols from East Asia: Insights gained from multiple observations and modeling. *Environmental Pollution*, *230*, 1030–1039. https://doi.org/10.1016/j.envpol.2017.07.062

Guo, S., Hu, M., Zamora, M. L., Peng, J., Shang, D., Zheng, J., et al. (2014). Elucidating severe urban haze formation in China. *Proceedings of the National Academy of Sciences*, *111*(49), 17,373–17,378. https://doi.org/10.1073/pnas.1419604111

He, C., Liu, R., Wang, X., Liu, S. C., Zhou, T., & Liao, W. (2019). How does El Niño-Southern Oscillation modulate the interannual variability of winter haze days over eastern China? *Science of the Total Environment*, *651*(Pt2), 1892–1902. https://doi.org/10.1016/j.scitotenv.2018.10.100

He, K. B., Jia, Y., Ma, Y., Lei, Y., Zhao, Q., Tanaka, S., & Okuda, T. (2009). Regionality of episodic aerosol pollution in Beijing. *Acta Scientiae Circumstantiae* (in Chinese), *29*(3), 482–487.

Hoffmann, P., & HeinkeSchlünzen, K. (2013). Weather pattern classification to represent the urban heat island in present and future climate. *Journal of Applied Meteorology and Climatology*, *52*(12), 2699–2714. https://doi.org/10.1175/JAMC-D-12-065.1

Hou, X., Zhu, B., Kumar, K. R., & Lu, W. (2019). Inter-annual variability in fine particulate matter pollution over China during 2013–2018: Role of meteorology. *Atmospheric Environment*, *214*, 116,842.

Hu, M., Jia, L., Wang, J., & Pan, Y. (2013). Spatial and temporal characteristics of particulate matter in Beijing, China using the empirical mode decomposition method. *Science of the Total Environment*, *458–460*, 70–80. https://doi.org/10.1016/j.scitotenv.2013.04.005

Huang, R. J., Zhang, Y., Bozzetti, C., Ho, K., Cao, J., Han, Y., et al. (2014). High secondary aerosol contribution to particulate pollution during haze events in China. *Nature*, *514*(7521), 218–222. https://doi.org/10.1038/nature13774

Huang, X., Wang, Z., & Ding, A. (2018). Impact of aerosol-PBL interaction on haze pollution: Multiyear observational evidences in North China. *Geophysical Research Letters*, *45*, 8596–8603. https://doi.org/10.1029/2018GL079239

Huth, R. (1996). Properties of the circulation classification scheme based on the rotated principal component analysis. *Meteorology and Atmospheric Physics*, *59*(3), 217–233. https://doi.org/10.1007/BF01030145

Huth, R. (2000). A circulation classification scheme applicable in GCM studies. *Theoretical and Applied Climatology*, *67*(1), 1–18. https://doi.org/10.1007/s007040070012

Huth, R., Beck, C., & Kučerová, M. (2016). Synoptic-climatological evaluation of the classifications of atmospheric circulation patterns over Europe. *International Journal of Climatology*, *36*(7), 2710–2726. https://doi.org/10.1002/joc.4546

Huth, R., Beck, C., Philipp, A., Demuzere, M., Ustrnul, Z., Cahynova, M., et al. (2008). Classifications of atmospheric circulation patterns: Recent advances and applications. *Annals. New York Academy of Sciences*, *1146*, 105–152. https://doi.org/10.1196/annals.1446.019

Jacobeit, J. (2010). Classifications in climate research. *Physics and Chemistry of the Earth*, *35*, 411–421. https://doi.org/10.1016/j.pce.2009.11.010

Jin, Y., Andersson, H., & Zhang, S. (2016). Air Pollution Control Policies in China: A retrospective and prospects. *International Journal of Environmental Research*. https://doi.org/10.3390/ijerph13121219

Kalkstein, L. S., & Corrigan, P. (1986). A synoptic climatological approach for geographical analysis: Assessment of sulfur dioxide concentrations. *Annals of the Association of American Geographers*, *76*, 381–395. https://doi.org/10.1111/j.1467-8306.1986.tb00126.x

Kalnay, E., Kanamitsu, M., Kistler, R., Collins, W., Deaven, D., Gandin, L., et al. (1996). The NCEP/NCAR 40- year reanalysis project. *Bulletin of the American Meteorological Society*, *77*(3), 437–471.

Kang, H., Zhu, B., Gao, J., He, Y., Wang, H., Su, J., et al. (2019). Potential impacts of cold frontal passage on air quality over the Yangtze River Delta, China. *Atmospheric Chemistry and Physics*, *19*(6), 3673–3685. https://doi.org/10.5194/acp-19-3673-2019

Li, J., Liao, H., Hu, J., & Li, N. (2019). Severe particulate pollution days in China during 2013–2018 and the associated typical weather patterns in Beijing-Tianjin-Hebei and the Yangtze River Delta regions. *Environmental Pollution*, *248*, 74–81. https://doi.org/10.1016/j.envpol.2019.01.124

Li, Z., Chen, H., Cribb, M., Dickerson, R., Holben, B., Li, C., et al. (2007). Preface to special section on East Asian studies of tropospheric aerosols: An international regional experiment (EAST-AIRE). *Journal of Geophysical Research*, *112*, D22S00. https://doi.org/10.1029/2007JD008853

Liu, Y., He, J., Lai, X., Zhang, C., & Che, H. (2020). Influence of atmospheric circulation on aerosol and its optical characteristics in the pearl river delta region. *Atmosphere*, *11*(3), 288. https://doi.org/10.3390/atmos11030288

Lyons, W. F., & Bonell, M. (1994). Regionalization of daily mesoscale rainfall in the tropical wet/dry climate of the townsville area of north-east queensland during the 1988–1989 wet season. *International Journal of Climatology*, *14*(2), 135–163. https://doi.org/10.1002/joc.3370140203

Ma, X. C., Wu, H., Ji, L., Zhang, Q., Huang, M., Li, H., et al. (2011). Vertical distributions of aerosols under different weather conditions in Beijing. *Meteorological monthly* (in Chinese), *37*(9), 1126–1133.

McGregor, G. R., & Bamzelis, D. (1995). Synoptic typing and its application to the investigation of weather air pollution relationships, Birmingham, United Kingdom. *Theoretical and Applied Climatology*, *51*, 223–236. https://doi.org/10.1007/BF00867281

Miao, Y., Guo, J., Liu, S., Liu, H., Li, Z., Zhang, W., & Zhai, P. (2017). Classification of summertime synoptic patterns in Beijing and their associations with boundary layer structure affecting aerosol pollution. *Atmospheric Chemistry and Physics*, *17*, 3097–3110. https://doi.org/10.5194/acp-17-3097-2017

Miao, Y., Liu, S., Sheng, L., Huang, S., & Li, J. (2019). Influence of boundary layer structure and low-level jet on $PM_{2.5}$ pollution in Beijing: A case study. *International Journal of Environmental Research and Public Health*, *16*, 616. https://doi.org/10.3390/ijerph16040616

Ning, G., Yim, S. H. L., Wang, S., Duan, B., Nie, C., Yang, X., et al. (2019). Synergistic effects of synoptic weather patterns and topography on air quality: A case of the Sichuan Basin of China. *Climate Dynamics*, *53*(11), 6729–6744. https://doi.org/10.1007/s00382-019-04954-3

Pasch, A., MacDonald, C., Gilliam, R., Knoderer, C., & Roberts, P. (2011). Meteorological characteristics associated with $PM_{2.5}$ air pollution in Cleveland, Ohio, during the 2009–2010 Cleveland multiple air pollutants study. *Atmospheric Environment*, *45*, 7026–7035. https://doi.org/10.1016/j.atmosenv.2011.09.065

Philipp, A., Bartholy, J., Beck, C., Erpicum, M., Esteban, P., Fettweis, X., et al. (2010). COST733CAT-a database of weather and circulation type classifications. *Physics and Chemistry of the Earth*, *35*, 360–373. https://doi.org/10.1016/j.pce.2009.12.010

Philipp, A., Beck, C., Esteban, P., Kreienkamp, F., Krennert, T., Lochbihler, K., et al. (2014). *cost733class-1.2 User Guide*. Augsburg.

Philipp, A., Beck, C., Huth, R., & Jacobeit, J. (2016). Development and comparison of circulation type classifications using the COST733 dataset and software. *International Journal of Climatology*, *36*, 2673–2691. https://doi.org/10.1002/joc.3920

Ren, Z. H., Su, F., Chen, Z., Hong, Z., Cheng, S., Gao, Q., & Feng, L. (2008). Influence of synoptic systems on the distribution and evolution process of PM_{10} concentration in the boundary layer in summer and autumn Chinese. *Journal of Atmospheric Sciences (in Chinese)*, *32*(4), 741–751.

Shahgedanova, M., Burt, T., & Davies, T. (1998). Synoptic climatology of air pollution in Moscow. *Theoretical and Applied Climatology*, *61*, 85–102. https://doi.org/10.1007/s007040050054

Shang, K. Z., Da, C., Fu, Y., Wang, S., & Yang, D. (2001). The stable energy in Lanzhou City and the relations between air pollution and it. *Plateau Meteorology (in Chinese)*, *20*(1), 76–81. https://doi.org/10.3321/j.issn:1000-0534.2001.01.013

Tai, A., Mickley, L., & Jacob, D. (2012). Impact of 2000-2050 climate change on fine particulate matter ($PM_{2.5}$) air quality inferred from a multi-model analysis of meteorological modes, Atmos. *Chemical Physics*, *12*, 11,329–11,337. https://doi.org/10.5194/acp-12-11329-2012

Tian, S., Pan, Y., Liu, Z., Wen, T., & Wang, Y. (2014). Size-resolved aerosol chemical analysis of extreme haze pollution events during early 2013 in urban Beijing, China. *Journal of Hazardous Materials*, *279*, 452–460. https://doi.org/10.1016/j.jhazmat.2014.07.023

Wang, B., Wu, Z. W., Chang, C.-P., Liu, J., Li, J. P., & Zhou, T. J. (2010). Another look at interannual-to-Interdecadal variations of the East Asian winter monsoon: The northern and southern temperature modes. *Journal of Climate*, *23*(6), 1495–1512. https://doi.org/10.1175/2009JCLI3243.1

Wang, J., He, R., Li, L., & Zhang, L. (2015). Characteristics and formation mechanism of a heavy air pollution episode in Shanghai. *Acta Scientiae Circumstantiae*, (in Chinese), *35*(5), 1537–1546.

Wang, L., & Chen, W. (2010). How well do existing indices measure the strength of the East Asian winter monsoon? *Advances in Atmospheric Sciences*, *27*, 855–870. https://doi.org/10.1007/s00376-009-9094-3

Wang, S. X., Zhao, B., Cai, S. Y., Klimont, Z. C., Nielsen, P., Morikawa, T., et al. (2014). Emission trends and mitigation options for air pollutants in East Asia. *Atmospheric Chemistry and Physics*, *14*, 6571–6603. https://doi.org/10.5194/acp-14-6571-2014

Wang, X., & Zhang, R. (2020). Effects of atmospheric circulations on the interannual variationin $PM_{2.5}$ concentrations over the Beijing–Tianjin–Hebeiregion in 2013–2018. *Atmospheric Chemistry and Physics*, *20*, 7667–7682. https://doi.org/10.5194/acp-20-7667-2020

Wang, Y., Wan, Q., Meng, W., Liao, F., Tan, H., & Zhang, R. (2011). Long impact of aerosols on precipitation and lightning over the Pearl River Delta megacity area in China. *Atmospheric Chemistry and Physics*, *11*, 12,421–12,436. https://doi.org/10.5194/acp-11-12421-2011

Wang, Y., Yao, L., Wang, L., Liu, Z., Ji, D., Tang, G., et al. (2014). Mechanism for the formation of the January 2013 heavy haze pollution episode over central and eastern China. *Science China Earth Sciences*, *57*, 14–25. https://doi.org/10.1007/s11430-013-4773-4

Wang, Y., Zhang, R., & Saravanan, R. (2014). Asian pollution climatically modulates midlatitude cyclones following hierarchical modelling and observational analysis. *Nature Communications*, *5*, 3098. https://doi.org/10.1038/ncomms4098

White, D., Richman, M., & Yarnal, B. (1991). Climate regionalization and rotation of principal components. *International Journal of Climatology*, *11*(1), 1–25. https://doi.org/10.1002/joc.3370110102

Wu, J., Li, G., Cao, J., Bei, N., Wang, Y., Feng, T., et al. (2017). Contributions of trans-boundary transport to summertime air quality in Beijing China. *Atmospheric Chemistry and Physics*, *17*(3), 2035–2051. https://doi.org/10.5194/acp-17-2035-2017

Wu, M., Luo, Y., Wu, D., Zeng, Z., & Fan, S. (2019). Influence of vertical temperature structure on air quality over Pearl River Delta region during dry season. *Environmental Science & Technology* (in Chinese), *42*(5), 189–195.

Xu, J. M., Chang, L., Ma, J., Mao, Z., Chen, L., & Cao, Y. (2016). Objective synoptic weather classification on PM2.5 pollution during autumn and winter seasons in Shanghai. *Acta Scientiae Circumstantiae* (in Chinese), *36*(12), 4303–4314. https://doi.org/10.13671/j.hjkxxb.2016.0224

Xu, X., Ding, G., Zhou, L., Zheng, X., Bian, L., Qiu, J., et al. (2003). Winter air pollution in Beijing: Chemical process regional three-dimensional structure characteristics. *Chinese Science Bulletin* (in Chinese), *48*(5), 496–501. https://doi.org/10.1007/BF03187060

Yang, X., Zhang, X., Kang, Y., Zhang, Y., Wang, S., Li, Z., & Li, H. (2017). Circulation weather type classification for air pollution over the Beijing-Tianjin-Hebei region during winter. *China Environmental Science* (in Chinese), *37*(9), 3201–3209.

Zhang, J. P., Zhu, T., Zhang, Q. H., Li, C. C., Shu, H. L., Ying, Y., et al. (2012). The impact of circulation patterns on regional transport pathways and air quality over Beijing and its surroundings. *Atmospheric Chemistry and Physics*, *12*, 5031–5053. https://doi.org/10.5194/acp-12-5031-2012

Zhang, R. H., Li, Q., & Zhang, R. N. (2014). Meteorological conditions for the persistent severe fog and haze event over eastern China in January 2013. *Science China: Earth Sciences* (in Chinese), *57*, 26–35. https://doi.org/10.1007/s11430-013-4774-3

Zhang, X. Y., Wang, J. Z., Wang, Y. Q., Liu, H. L., Sun, J. Y., & Zhang, Y. M. (2015). Changes in chemical components of aerosol particles in different haze regions in China from 2006 to 2013 and contribution of meteorological factors. *Atmospheric Chemistry and Physics*, *15*, 12,935–12,952. https://doi.org/10.5194/acp-15-12935-2015

Zhang, Y., Ding, A., Mao, H., Nie, W., Zhou, D., Liu, L., et al. (2016). Impact of synoptic weather patterns and inter-decadal climate variability on air quality in the North China Plain during 1980–2013. *Atmospheric Environment*, *124*, 119–128. https://doi.org/10.1016/j.atmosenv.2015.05.063

Zhao, X. J., Zhao, P. S., Xu, J., Meng, W., Pu, W. W., Dong, F., et al. (2013). Analysis of a winter regional haze event and its formation mechanism in the North China Plain. *Atmospheric Chemistry and Physics*, *13*, 5685–5696. https://doi.org/10.5194/acp-13-5685-2013

Zhao, Z. Q., Wei, Y., Zhang, X., Qin, W., & Xie, H. (2015). The correlation analysis of Nanjing haze days and meteorological factors. *China Environmental Science* (in Chinese), *35*(12), 3570–3580.

Zheng, G., Duan, F., Ma, Y., Zhang, Q., Huang, T., Kimoto, T., et al. (2016). Episode-based evolution pattern analysis of haze pollution: Method development and results from Beijing, China. *Environmental Science & Technology*, *50*(9), 4632–4641. https://doi.org/10.1021/acs.est.5b05593

Zheng, G. J., Duan, F. K., Su, H., Ma, Y. L., Cheng, Y., Zheng, B., et al. (2015). Exploring the severe winter haze in Beijing: The impact of synoptic weather, regional transport and heterogeneous reactions. *Atmospheric Chemistry and Physics*, *15*, 2969–2983. https://doi.org/10.5194/acp-15-2969-2015

Zhu, J., Liao, H., & Li, J. (2012). Increases in aerosol concentrations over eastern China due to the decadal-scale weakening of the East Asian summer monsoon. *Geophysical Research Letters*, *39*, L09809. https://doi.org/10.1029/2012GL051428